THE JOURNAL OF PHYSICAL CHEMISTRY LETTERS
A JOURNAL OF THE AMERICAN CHEMICAL SOCIETY

pubs.acs.org/JPCL
Letter

Biexciton and Singlet Trion Upconvert Exciton Photoluminescence in a $MoSe_2$ Monolayer Supported by Acoustic and Optical K-Valley Phonons

Joanna Jadczak,* Joerg Debus, Justyna Olejnik, Ching-Hwa Ho, Kenji Watanabe, Takashi Taniguchi, and Leszek Bryja

Cite This: *J. Phys. Chem. Lett.* 2023, 14, 8702−8708
Read Online
ACCESS | Metrics & More | Article Recommendations

ABSTRACT: Transition metal dichalcogenide monolayers represent unique platforms for studying both electronic and phononic interactions as well as intra- and intervalley exciton complexes. Here, we investigate the upconversion of exciton photoluminescence in $MoSe_2$ monolayers. Within the nominal transparency window of $MoSe_2$ the exciton emission is enhanced for resonantly addressing the spin-singlet negative trion and neutral biexciton at a few tens of meV below the neutral exciton transition. We identify that the A'_1 optical phonon at the K valley provides the energy gain in the upconversion process at the trion resonance, while ZA(K) phonons with their spin- and valley-switching properties support the biexciton driven upconversion of the exciton emission. Interestingly, the latter upconversion process yields unpolarized exciton photoluminescence, while the former also leads to circularly polarized emission. Our study highlights high-order exciton complexes interacting with optical and acoustic K-valley phonons and upconverting light into the bright exciton.

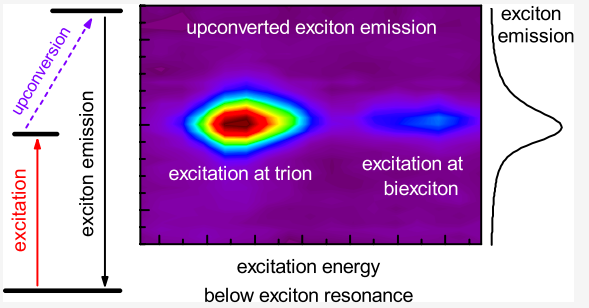

Transition metal dichalcogenide (TMDC) monolayers are direct band gap semiconductors with unique optical and spin-valley properties.[1] Their two-dimensional (2D) nature and the reduced dielectric screening of the Coulomb interaction allow for the formation of excitons with a binding energy of hundreds of meV[2,3] and high-order excitonic complexes, such as trions and biexcitons with binding energies of tens of meV.[4−12] Moreover, due to the strong spin−orbit coupling in TMDC monolayers and the resulting valley-contrasting spin splitting at the K valleys, the excitonic complexes possess both the spin as well as valley degree of freedom.[1]

In optically darkish systems, such as WS_2 and WSe_2 monolayers, the electric-dipole forbidden (optically dark) exciton state is positioned at lower energy than the optically active exciton state. On the contrary, in $MoSe_2$ monolayers the bright exciton state is at the lowest energy. These level hierarchies as well as exciton−phonon interactions were studied due to the progress in elaborating high-quality hBN-encapsulated TMDC monolayers.[13] In this context, upconversion photoluminescence (PL) spectroscopy recently provided thorough insights into exciton−exciton and exciton−phonon interactions and was successfully employed to reveal the coupling between various excitonic complexes in the optically darkish hBN-encapsulated WSe_2 and WS_2 monolayers. In particular, upconversion of light from dark excitons, trions, and biexcitons to bright excitons was observed.[14−16]

In the n-type $MoSe_2$ monolayer, the lowest energy trion configuration is the negative intervalley spin-singlet state (T_S). Interestingly, the T_S state typically dominates the PL spectra in $MoSe_2$ monolayers at low temperatures but is dramatically weakened with increasing temperature. In contrast to that, in $Mo(S_ySe_{1-y})_2$ alloys with a sulfur mole content up to $y = 0.5$, the trion emission is also robust at elevated temperatures.[8] This observation was attributed to a strong increase in the exciton−trion coupling strength and to a rising 2D electron gas concentration caused by an increasing sulfur content.[8] The enhanced exciton−trion coupling was realized by tuning phonon energies to the trion binding energy in the $Mo(S_ySe_{1-y})_2$ alloys. Also, the coherent and incoherent nature of the exciton−trion coupling and relevant time scales in $MoSe_2$ monolayers were revealed by optical 2D coherent spectroscopy; it demonstrated an efficient energy transfer via

Received: July 17, 2023
Accepted: September 18, 2023
Published: September 21, 2023

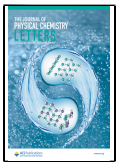

https://doi.org/10.1021/acs.jpclett.3c01982
J. Phys. Chem. Lett. 2023, 14, 8702−8708

phonon-assisted exciton-to-trion downconversion within 2−3 ps and trion-to-exciton upconversion in 8 ps.[17] The exciton−trion interaction in TMDC monolayers may be alternatively probed in upconversion (UPC) PL experiments.[14,18] The excess energy required for the UPC process may be taken from phonons or resident electrons in the monolayer.[15] Hence, the UPC PL provides information on both the energy spectra of the TMDCs as well as the scattering mechanism related to exciton−exciton, exciton−electron, and exciton−phonon interactions.

Here, we probe the upconversion photoluminescence in an optically bright hBN-encapsulated $MoSe_2$ monolayer system. UPC PL excitation reveals two pronounced resonances below the neutral 1s A-exciton (X). The resonance detected at an energy of about 25 meV below X coincides with the PL peak and binding energy of the singlet trion T_S. The second resonance at −18 meV with respect to the exciton transition is attributed to the neutral biexciton (XX^0), which was previously identified in a $MoSe_2$ monolayer using polarization-resolved 2D coherent spectroscopy.[10] We propose that the energy gains required in the UPC of the exciton PL originate from different interactions, including optical or acoustic phonons at the K valley. The upconversion of light from T_S and XX^0 into X is observed only for samples with a relatively weak electron concentration and is enhanced at elevated temperatures. We also evaluate the UPC as a function of the incident laser power and demonstrate specific polarization characteristics of the upconverted exciton emission. In contrast to tungsten-based structures, probing of upconverted exciton PL in $MoSe_2$ requires a low number of resident electrons and is realized only in hBN-encapsulated samples. Moreover, as biexcitons are challenging to be identified unambiguously using linear optical spectroscopy methods and were detected only in WS_2 and WSe_2 monolayers so far in regular PL experiments, upconversion is an alternative route to address, for example, biexcitons in TMDC monolayers, particularly in $MoSe_2$. UPC further provides information on the energies of bound carrier complexes in TMDCs and scattering processes related to exciton−electron and exciton−phonon interactions.

In Figure 1a, intensity normalized PL spectra are shown for an uncapped $MoSe_2$ monolayer placed on an hBN substrate ($MoSe_2$/hBN) and for an hBN-encapsulated $MoSe_2$ monolayer (hBN/$MoSe_2$/hBN). The spectra were measured at 7 K and were excited nonresonantly by laser light having an energy of 2.33 eV. Since the energy E_X of the exciton PL peak changes from flake to flake between 1.627 and 1.638 eV, the energy scale of each spectrum is referred to the exciton energy; accordingly, the energy difference $E - E_X$ is chosen for the horizontal axis. The predominant peak which is about 26 or 30 meV below the exciton PL peak is attributed to the spin-singlet negative trion T_S whose binding energy lies in this energy range.[5] While the neutral exciton recombination in $MoSe_2$ yields a symmetric peak, the trion PL is asymmetric with a broad low-energy flank which is attributed to an electron recoil effect for trions.[19] The doping level of the samples could be estimated by the intensities and relative energy positions ΔE_{X-T} of the exciton and trion PL peaks. On the one hand, the X emission intensity in the $MoSe_2$/hBN structure is significantly lower than that in the hBN/$MoSe_2$/hBN sample and, on the other hand, ΔE_{X-T} amounts to 30 and 26 meV, respectively. These differences indicate a higher electron density in the uncapped structure. On the basis of the exciton−trion energy splittings ΔE_{X-T} and gate-dependent

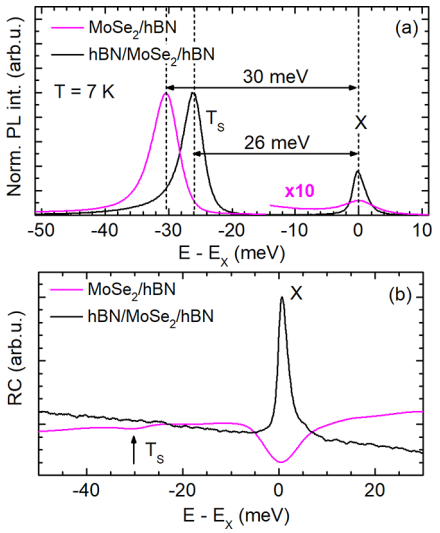

Figure 1. (a) PL spectra of $MoSe_2$/hBN and hBN/$MoSe_2$/hBN van der Waals heterostructures measured at T = 7 K. The energy splitting between the exciton and singlet trion PL lines is marked by a horizontal arrow. (b) RC spectra for both structures measured at 7 K.

optical characteristics of $MoSe_2$,[20] we estimate the electron density to be about 2×10^{10} cm^{-2} in the encapsulated monolayer, whereas in the uncapped monolayer it is in the order of 10^{12} cm^{-2}. Additionally, in Figure 1b we compare the reflectance contrast (RC) spectra of both samples excited by white light. As clearly seen, only for $MoSe_2$/hBN a weak negative trion resonance is resolved, which underlines the presence of a significant electron doping.[20] For hBN/$MoSe_2$/hBN, the exciton resonance is sharp and intense due to the low electron doping level and the encapsulation, which protects the monolayer from charge transfers and local electric field fluctuations.

We now focus on the upconversion of the neutral exciton PL in the $MoSe_2$ monolayer, for excitation energies below the neutral exciton in the nominal $MoSe_2$ transparency range, and demonstrate its dependence on variations of the temperature, laser power, and polarization. In the following, we present the data for the hBN/$MoSe_2$/hBN heterostructure. For the $MoSe_2$/hBN structure, we observed only negligibly weak upconverted X PL.

The regular and upconverted PL of the hBN/$MoSe_2$/hBN structure recorded at 7 K is demonstrated in Figure 2. In Figure 2a, the PL spectrum and the energy range that is resonantly excited for the UPC PL are shown. The latter marked by vertical arrows goes from about −15 meV to the low-energy flank of the trion PL at about −29 meV. For a UPC photoluminescence excitation (PLE) spectrum, the neutral exciton PL is monitored during the variation of the laser excitation energy E_{exc}. The color map in Figure 2b displays the UPC PLE spectra as a function of the excitation energy detuned from E_X, while the integrated exciton UPC PL $I_{X,UPC}$ is shown in Figure 2c. The UPC energy gain is given by the energy difference $|E_{exc} - E_X|$. Both the color map and the integrated exciton UPC PL clearly exhibit a prominent resonance at an energy gain of about 25 meV. This corresponds to the binding energy of the spin-singlet negative trion T_S. A second weak resonance is observed at an energy gain of about 18 meV. This enhancement of the exciton PL

https://doi.org/10.1021/acs.jpclett.3c01982
J. Phys. Chem. Lett. 2023, 14, 8702−8708

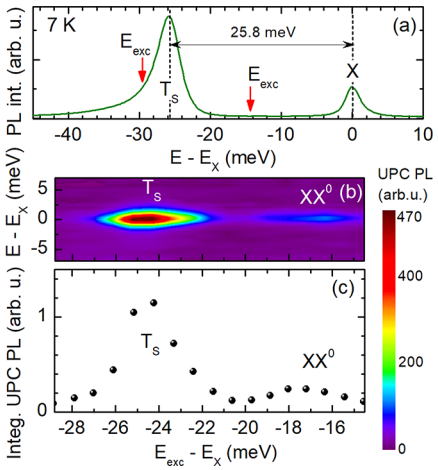

Figure 2. (a) PL spectrum of the hBN/$MoSe_2$/hBN structure detected at 7 K, for nonresonant laser excitation at 2.33 eV. (b) Color map of the UPC PLE spectra with a detection range of ±6 meV at exciton resonance E_X; T = 7 K. (c) Integrated UPC PL of the neutral exciton for excitation energies ranging from −29 to about −15 meV with respect to the X resonance.

may originate from the UPC process involving the neutral biexciton XX^0 whose binding energy lies in this range.[10]

In order to gain further insight into the exciton emission upconverted from the trion T_S and biexciton XX^0 we perform comparative temperature-dependent PL and UPC PLE measurements. In Figures 3a–f the PL spectra, the UPC PLE spectra, and the integrated UPC PL measured at 40 and 80 K are presented. At these temperatures, we tune the excitation energy through the biexciton and singlet trion resonances of the $MoSe_2$ monolayer, as marked by the red arrows in the PL spectra of panels a and b, and detect the response of the X emission. The resulting UPC PLE spectra are shown in panels c and d, and the integrated UPC PL $I_{X,UPC}$ of the X is presented in panels e and f. Additionally, Figure 3g provides an overview about the integrated intensities of the X and T_S PL peaks (black symbols) and the integrated X PL upconverted from the XX^0 and T_S states (red symbols) as a function of temperature from 7 to 80 K. Up to 50 K, the PL intensity of the negative trion exceeds that of the exciton, while both lines become weaker with increasing temperature. By comparison, the upconverted X PL is enhanced with rising temperature: $I_{X,UPC}$ is maximum at about 50 K, for resonantly exciting T_S, and is reduced by further increasing the temperature. For exciting XX^0, $I_{X,UPC}$ exhibits a maximum at about 60 K. This thermal behavior differs from that observed in WS_2 monolayers,[16,18] where the upconverted PL of the exciton becomes significantly intensified with rising temperature and even exceeds the regular PL intensity.

We further study the dependence of the upconverted X PL on the incident laser power P. It will provide insight into the character of the UPC resonances, in addition to the prior assignment of the resonances according to the binding energies of the negative trion and neutral biexciton. Typical UPC PLE spectra recorded for 10, 6, and 4 mW are depicted in Figure 4a,b,c, respectively. The evolution of the integrated UPC exciton PL as a function of P, for resonantly addressing the negative trion and biexciton, is given in panel d using a double-logarithmic presentation. $I_{X,UPC}$ depends nonlinearly on the laser power which is evaluated from the slopes α of 2.08 and 1.66, for exciting the XX^0 and T_S resonances, respectively. The practically quadratic power dependence (α_{XX^0} = 2.08) of $I_{X,UPC}$, for $E_{exc} - E_X = -18$ meV, characterizes a process in which a biexciton is involved. The power-dependent evolution of the X PL intensity upconverted from T_S is described by α_{T_S} = 1.66, which reflects the power-dependent slope of the trion regular PL intensity.[21]

Finally, we elucidate the polarization properties of the exciton PL upconverted from the negative trion and neutral biexciton states, yielding additional details on the UPC mechanisms, which are discussed in the following section. In Figure 4e the UPC PLE spectra are demonstrated for linearly polarized excitation and unpolarized detection, while in Figure 4f,g the incident light and the emission are cocircularly and cross-circularly polarized, respectively. Figure 4h displays $I_{X,UPC}$ as a function of the polarization configurations for excitation energies ranging from −28 to −14 meV in proximity to the X. The upconverted X PL is predominantly unpolarized, for

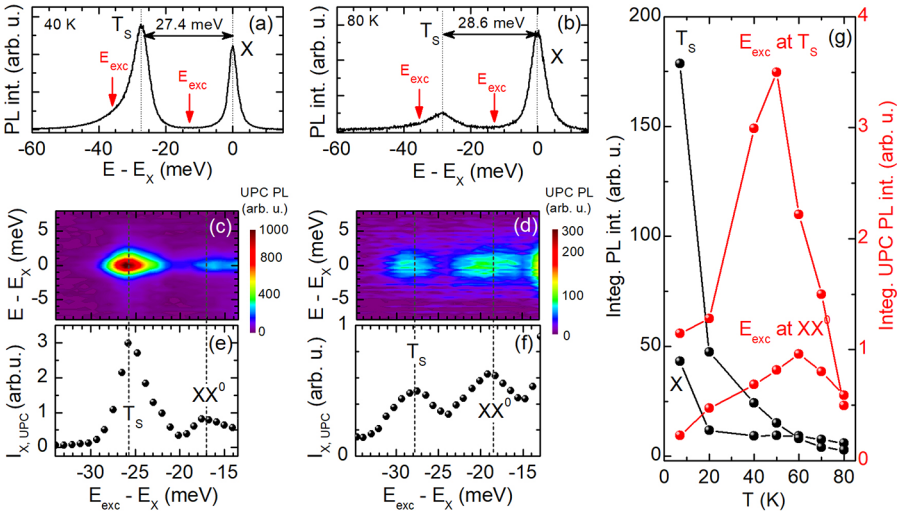

Figure 3. PL spectra of the hBN-encapsulated $MoSe_2$ monolayer recorded at (a) 40 and (b) 80 K. Color maps of the UPC PLE spectra for varying energy gain measured at (c) 40 and (d) 80 K. (e and f) Integrated UPC PL of X as a function of the energy gain given at 40 and 80 K, respectively. (g) Temperature dependence of (left scale) integrated PL intensities and (right scale) $I_{X,UPC}$ excited at T_S and XX^0.

https://doi.org/10.1021/acs.jpclett.3c01982
J. Phys. Chem. Lett. 2023, 14, 8702−8708

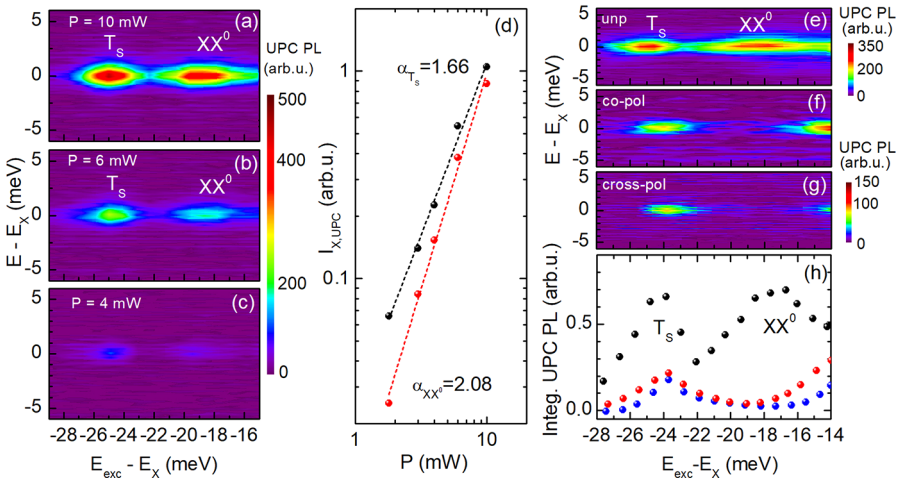

Figure 4. UPC PLE spectra as color maps obtained at (a) 10 mW, (b) 6 mW, and (c) 4 mW laser power. (d) The integrated UPC PL of the exciton is shown as a function of the laser power, for addressing the XX^0 (red circles) and T_S (black circles). (e–g) Unpolarized and circular-polarization resolved UPC PLE spectra measured at 7 K and P = 8 mW. The color scale at the top right belongs to panel e; the bottom-right scale refers to panels f and g. (h) Integrated UPC PL of X as a function of the energy gain, for the different polarization configurations. The black colored data points represent the unpolarized case, while the red (blue) symbols display the copolarized (cross-polarized) configuration.

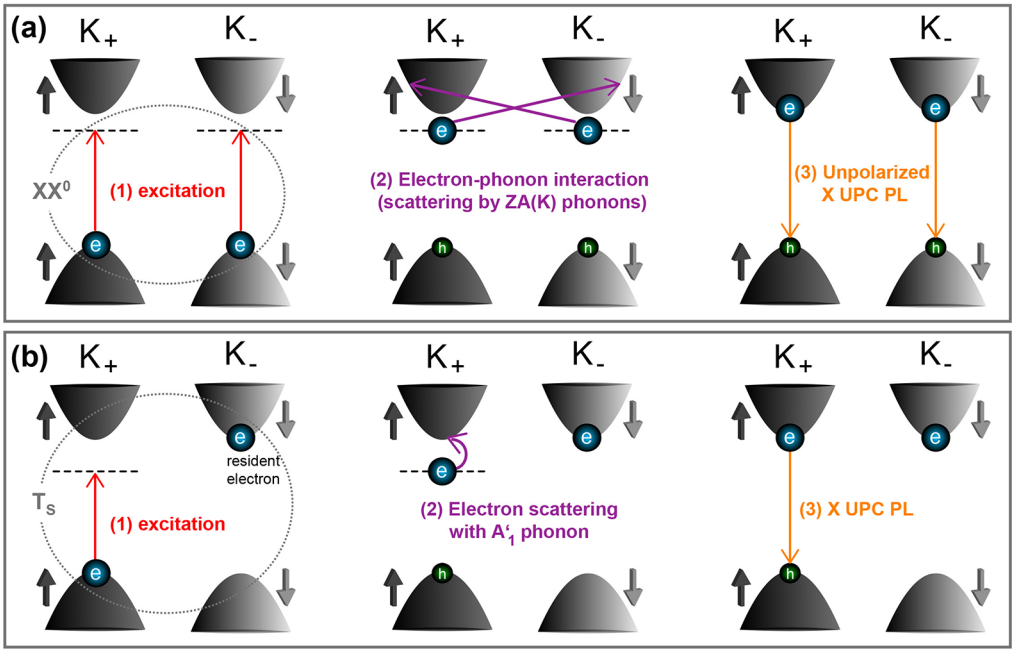

Figure 5. Schematic presentation of the mechanisms for upconverting the exciton PL by the (a) neutral biexciton and (b) spin-singlet trion. Each UPC process is sequentially sketched by going from the left to the right side. The single-particle picture is chosen where an electron (a hole) is illustrated by a blue (green) sphere. Only the energetically lowest conduction subband and highest valence subband are shown.

tuning the excitation energy to the biexciton resonance, while in the circularly polarized spectra $I_{X,UPC}$ is negligibly weak. By comparison, the exciton PL upconverted from the negative trion T_S is slightly polarized (+10%) with regard to the laser light polarization, while its intensity is also high in the unpolarized configuration. It is worthwhile to mention that $I_{X,UPC}$ becomes significantly polarized (+50%) for reducing the energy gain to 14 meV. It is consistent with results obtained for the regular exciton PL whose circular polarization is rather low compared to other TMDCs[22] and is enhanced for approaching the excitation energy of the A-exciton resonance.[23,24]

The experimental observations performed in the nominal transparency window of $MoSe_2$ are summarized in the following: (a) only the hBN-encapsulated $MoSe_2$ monolayer exhibits pronounced UPC PL of the neutral exciton (1s A-exciton); (b) the X PL is enhanced for resonantly addressing the spin-singlet negative trion at an energy gain of about 25 meV and the neutral biexciton at about 18 meV; (c) the UPC PL possesses intensity maxima at elevated temperatures; (d) the UPC PL intensity is scaled nonlinearly with the incident laser power; and (e) the UPC PL of the exciton is clearly unpolarized at the XX^0 resonance and exhibits a slightly positive circular polarization at the T_S resonance.

In contrast to WSe_2 and WS_2 monolayers in which the lowest exciton state is optically forbidden (spin-dark)[25] at the K valleys, $MoSe_2$ monolayers are characterized by spin-allowed

https://doi.org/10.1021/acs.jpclett.3c01982
J. Phys. Chem. Lett. 2023, 14, 8702−8708

neutral excitons as energetically lowest states at the K_+ and K_- valleys. The bright exciton at the K_+ (K_-) valley is excited by σ^+ (σ^-) circularly polarized light in accordance with a valley index of either +1 or −1. Here, the upconversion of the exciton emission is initiated by optically creating either the neutral biexciton XX^0 or the negative trion T_S. The difference between the neutral exciton energy and the incident laser light energy corresponds to the binding energy of the excitonic complex involved in the UPC process. An individual number of interactions is followed by the final exciton annihilation. The overall efficiency of the UPC is governed by the order of the process, whereby spin- and momentum-conserving scattering or exchange interaction processes are favored.

We first consider the exciton PL UPC involving the neutral biexciton which is observed at an optical excitation energy of about ΔE_{XX^0} = 18 meV below the X transition (corresponding to the XX^0 binding energy) and in the presence of only a low number of resident electrons (close to the neutrality point). Moreover, the energy difference (energy gain) lies within the range of phonon energies, and the UPC is particularly pronounced at elevated temperatures. These aspects indicate the significance of phonon contributions without a disturbing impact of additional electrons (due to, e.g., exchange interaction). Additionally, the quadratic power dependence is also characteristic for neutral biexcitons. Besides the specific temperature dependence and low energy gain, the strong nonlinear power dependence rules out a potential two-photon absorption with a real biexciton state and an Auger-like process, as demonstrated by ref 26. As shown in Figure 5a, we thus propose that initially (1) a neutral biexciton with spin-up electron and hole at the K_+ and spin-down electron and hole at the K_- valley are excited, whereby the net angular momentum transfer is zero, in agreement with the linearly polarized incident light. Afterward, (2) each electron interacts with the zone-corner flexural acoustic ZA(K) phonon mode of about E_{ZA} = 17.5 meV (4.2 THz) energy.[27] Hence, each electron is scattered to the opposite valley ($K_+ \rightarrow K_-$, $K_+ \rightarrow K_-$),[28] under reversal of its spin so that in total the spin angular momentum is not changed and the crystal momentum is conserved. In accordance with the Elliot−Yafet mechanism the phonon in the spin-flip process must possess an odd parity under mirror-symmetry operation.[29] In contrast to the longitudinal and transversal acoustic phonon modes, the ZA(K) phonon fulfills this criterion.[27] The phonon absorption provides the energy $2E_{ZA}$ to the carrier complex which is about twice the binding energy ($2\Delta E_{XX^0}$). Therefore, we propose that after the electron−phonon interaction, the electrons relax to the minimum of their conduction sub-bands, as sketched in the right scheme of Figure 5a. The electron−phonon interaction with the subsequent electron relaxation adds dispersion to the resonance energy so that from about $E_{exc} - E_X = -20$ meV until −16 meV the XX^0 resonance is observed. Finally, (3) both excitons recombine, giving rise to emission which is unpolarized. Since the upconverted X PL is not observed in any circular polarization setting of the detection path, for linearly polarized excitation, we conclude that the final state composed of two bright excitons residing at the K_+ and K_- valleys is a coherent intervalley (superposition) state.

We take into account the neutral biexciton in $MoSe_2$ composed of two spin-allowed intravalley excitons residing at the K_+ and K_- valley, respectively. This intervalley XX^0 configuration is, due to Pauli blocking, energetically favored against an intravalley configuration in which a bright and dark exciton are both excited in the same valley.[11]

For the exciton emission upconverted from the spin-singlet trion, we propose the following spin-conserving process. As shown in Figure 5b, for σ^+ polarized excitation and detection, (1) the T_S state is excited with a spin-up electron and hole at the K_+ valley as well as a spin-down resident electron at the K_- valley. (2) As only for low electron concentration the X PL is upconverted from T_S, we propose that the spin-up photoelectron is scattered by the A'_1 phonon to the energetically lowest subband at the K_+ valley. The A'_1 optical phonon at the K valleys has an energy of about 25 meV (6 THz),[27] which well fits to the T_S binding energy. While the resident electron remains at the spin-down subband of the K^- valley, the spin-up photoelectron as well as the hole at the K^+ valley recombine, resulting in σ^+ polarized exciton emission. The X PL upconverted from the negative trion is both copolarized as well as slightly cross-polarized. The cross-polarization may hint at a stimulated exciton (boson) scattering.[26] Alternatively, due to intervalley scattering of the hole including a spin reversal,[23] the recombination of the electron and hole at the K_- valley leads to σ^- polarized exciton emission which also explains the emission in the cross-polarized configuration.

The contribution of phonon modes to UPC processes in TMDCs strongly depends on temperature.[18,30] Recent theoretical calculations have shown that in $MoSe_2$ the upconversion rate is significantly higher than that in WSe_2.[30] It results in a stronger electron−phonon interaction and a shorter thermal average upconversion time, which is about eight times faster in $MoSe_2$ than in WSe_2.[30] Moreover, in a $MoSe_2$ monolayer the thermal average upconversion time decreases strongly with increasing temperature; at 60 K it is about 10 times smaller than at 7 K.[30] This thermal behavior supports the explanation of the temperature dependences observed in our experiments and the UPC mechanisms, including optical and zone-edge acoustic phonons. The temperature-dependent growth of the exciton UPC PL is likely governed by an increased phonon population, leading to a more probable phonon-mediated scattering of the electrons. By comparison, the thermally induced PL decrease in the $MoSe_2$ monolayer may be caused by an intravalley scattering with acoustic phonons.[31,32]

For an hBN-encapsulated $MoSe_2$ monolayer with a relatively low concentration of resident electrons (2×10^{10} cm^{-2}), we have demonstrated the upconversion of the 1s A-exciton PL by the neutral biexciton and singlet trion, respectively. In the nominal transparency window of $MoSe_2$ the X PL is observed for resonantly addressing T_S (XX^0) at an energy of about 25 meV (18 meV) below the neutral exciton resonance. The upconverted X PL is enhanced nonlinearly with the incident laser power and also at elevated temperatures of 50−60 K. The latter is attributed to an increased phonon population giving rise to a high phonon-mediated scattering rate of the electrons. Additionally, the UPC PL of the exciton is unpolarized at the XX^0 resonance and displays a slight circular polarization at the T_S resonance. The mechanism of the exciton PL upconverted by the neutral biexciton is attributed to the interaction of the photocreated electrons at the K_+ and K_- valleys with zone-corner flexural acoustic ZA(K) phonons. They scatter the electrons to opposite valleys under reversal of their spins. Finally, two bright excitons residing at the K_+ and K_- valleys recombine leading to unpolarized emission at the neutral exciton energy. The UPC of the X PL via the spin-singlet

https://doi.org/10.1021/acs.jpclett.3c01982
J. Phys. Chem. Lett. 2023, 14, 8702−8708

negative trion is assigned to a spin- and valley-conserving scattering process of the photocreated electron with the optical A'_1 phonon mode whose energy at the K valleys matches the energy difference between the singlet trion and the neutral exciton.

Our results extend the current discussion about interactions of electrons with both optical and acoustic phonons at the K valleys and their role in the upconversion of exciton emission in $MoSe_2$ monolayers. We also provide further insights into resonant exciton−trion and exciton−biexciton couplings for optically exciting a 2D material within its nominal transparency range.

MATERIALS AND METHODS

$MoSe_2$ crystals were grown by a chemical vapor transport technique. Prior to the crystal growth, the powdered compounds were prepared from the elements Mo (purity: 99.99%) and Se (99.999%) by reaction at 1000 °C for 10 days in quartz ampules. The mixture was slowly heated to 1000 °C. The chemical transport was achieved with I_2 as transport agent having a concentration of about 5 mg/cm^3. The growth temperature was gradually changed from 1030° to 980 °C, with a temperature gradient of 3 °C/cm and a growth time of 20 days. The crystals had the shape of thin-layered plates with thicknesses and surface areas ranging from 20 to 1000 μm and from 20 to 100 mm^2, respectively.

We prepared van der Waals hBN-encapsulated $MoSe_2$ heterostructures using high-purity hexagonal boron nitride (hBN) and Si substrates (300 nm SiO_2). The monolayers were mechanically exfoliated from the $MoSe_2$ bulk crystals using the deterministic all-dry stamping method, similar to Castellanos-Gomez et al.[33] A $MoSe_2$ monolayer and hBN crystals were first exfoliated on a flexible PDMS gel-film stamp rigidly attached to a glass slide. The thicknesses of the hBN flakes were about 200 nm for the bottom layer in $MoSe_2$/hBN structures and about 100 nm for the bottom layer and about 2 nm for the top layer, respectively, in hBN-encapsulated structures. During the transfer process, the substrate and the stamp were placed below an optical microscope equipped with an XYZ positioning stage. A long-working distance microscope objective enabled us to locate and deterministically transfer selected flakes to the substrate. After each transfer step the sample was heated to about 180 °C for 20 min in air. After the last layer was added to the sample, a final thermal annealing was performed in air for 2 h at about 200 °C.

For the PL and UPC PLE experiments, the samples were mounted on the coldfinger of a nonvibrating closed-cycle helium cryostat, in which the temperature could be varied from 7 to 350 K. The PL was excited by the second harmonic 532 nm (2.33 eV) of a continuous-wave single-mode Nd:YAG laser. The UPC PLE was excited by a continuous-wave Ti:sapphire laser whose emission was tunable in the range from 760 to 780 nm. The laser beam was focused on the sample under normal incidence using a high-resolution, long-working distance (WD = 10 mm, NA = 0.65) 50× microscope objective. The diameter of the excitation spot was about 1 μm. The emission from the sample was collected by the same microscope objective and was analyzed with a 0.5-m-focal length spectrometer equipped with a 600 lines/mm grating and a Peltier-cooled charged-coupled-device Si camera. The RC spectrum was measured at the same setup using a filament lamp as a light source. To eliminate the scattered laser light, a set of short- and long-pass edged filters was used. For the polarization-resolved experiments, a Glan-Thompson prism combined with a quarter-wave retardation plate was introduced in the excitation and detection path.

AUTHOR INFORMATION

Corresponding Author

Joanna Jadczak − *Department of Experimental Physics, Wrocław University of Science and Technology, 50-370 Wrocław, Poland;* orcid.org/0000-0003-2953-1203; Email: joanna.jadczak@pwr.edu.pl

Authors

Joerg Debus − *Department of Physics, TU Dortmund University, 44227 Dortmund, Germany;* orcid.org/0000-0002-8678-4402

Justyna Olejnik − *Department of Experimental Physics, Wrocław University of Science and Technology, 50-370 Wrocław, Poland;* orcid.org/0009-0007-4948-4789

Ching-Hwa Ho − *Graduate Institute of Applied Science and Technology, National Taiwan University of Science and Technology, Taipei 106, Taiwan;* orcid.org/0000-0002-7195-208X

Kenji Watanabe − *National Institute for Materials Science, Tsukuba, Ibaraki 305-0044, Japan;* orcid.org/0000-0003-3701-8119

Takashi Taniguchi − *National Institute for Materials Science, Tsukuba, Ibaraki 305-0044, Japan;* orcid.org/0000-0002-1467-3105

Leszek Bryja − *Department of Experimental Physics, Wrocław University of Science and Technology, 50-370 Wrocław, Poland*

Complete contact information is available at: https://pubs.acs.org/10.1021/acs.jpclett.3c01982

Notes

The authors declare no competing financial interest.

ACKNOWLEDGMENTS

The project was funded by the QuanterERA II European Union's Horizon 2020 research and innovation programme under the EQUAISE project, Grant Agreement No. 101017733, under the supervision of the National Center for Research and Development in Poland within the project QuantERA II ERA-Net Cofund in Quantum Technologies (QUANTERAII/1/74/EQUAISE/2022). J.D. acknowledges the support by the DFG-funded TRR 160 (Project B4, No. 249492093).

REFERENCES

(1) Xiao, D.; Liu, G.-B.; Feng, W.; Xu, X.; Yao, W. Coupled Spin and Valley Physics in Monolayers of MoS_2 and Other Group-VI Dichalcogenides. *Phys. Rev. Lett.* **2012**, *108*, 196802.

(2) Mak, K. F.; Lee, C.; Hone, J.; Shan, J.; Heinz, T. F. Atomically Thin MoS_2: A New Direct-Gap Semiconductor. *Phys. Rev. Lett.* **2010**, *105*, 136805.

(3) Wang, G.; Chernikov, A.; Glazov, M. M.; Heinz, T. F.; Marie, X.; Amand, T.; Urbaszek, B. Colloquium: Excitons in Atomically Thin Transition Metal Dichalcogenides. *Rev. Mod. Phys.* **2018**, *90*, 021001.

(4) Drüppel, M.; Deilmann, T.; Krüger, P.; Rohlfing, M. Diversity of trion states and substrate effects in the optical properties of an MoS_2 monolayer. *Nat. Commun.* **2017**, *8*, 2117.

(5) Mostaani, E.; Szyniszewski, M.; Price, C. H.; Maezono, R.; Danovich, M.; Hunt, R. J.; Drummond, N. D.; Fal'ko, V. I. Diffusion quantum Monte Carlo study of excitonic complexes in two-

https://doi.org/10.1021/acs.jpclett.3c01982
J. Phys. Chem. Lett. 2023, 14, 8702−8708

dimensional transition-metal dichalcogenides. *Phys. Rev. B* **2017**, *96*, 075431.
(6) Vaclavkova, D.; Wyzula, J.; Nogajewski, K.; Bartos, M.; Slobodeniuk, A. O.; Faugeras, C.; Potemski, M.; Molas, M. R. Singlet and Triplet Trions in WS_2 Monolayer Encapsulated in Hexagonal Boron Nitride. *Nanotechnology* **2018**, *29*, 325705.
(7) Jadczak, J.; Kutrowska-Girzycka, J.; Bieniek, M.; Kazimierczuk, T.; Kossacki, P.; Schindler, J. J.; Debus, J.; Watanabe, K.; Taniguchi, T.; Ho, C. H.; et al. Probing Negatively Charged and Neutral Excitons in MoS_2/hBN and hBN/MoS_2/hBN van der Waals Heterostructures. *Nanotechnology* **2021**, *32*, 145717.
(8) Jadczak, J.; Kutrowska-Girzycka, J.; Kapuściński, P.; Huang, Y. S.; Wójs, A.; Bryja, L. Probing of free and localized excitons and trions in atomically thin WSe_2, WS_2, $MoSe_2$ and MoS_2 in photoluminescence and reflectivity experiments. *Nanotechnology* **2017**, *28*, 395702.
(9) Grzeszczyk, M.; Olkowska-Pucko, K.; Nogajewski, K.; Watanabe, K.; Taniguchi, T.; Kossacki, P.; Babiński, A.; Molas, M. R. Exposing the Trion's Fine Structure by Controlling the Carrier Concentration in hBN-Encapsulated MoS_2. *Nanoscale* **2021**, *13*, 18726−18733.
(10) Hao, K.; Specht, J.; Nagler, P.; Xu, L.; Tran, K.; Singh, A.; Chandriker, K.; Schuller, C.; Korn, T.; Richter, M.; et al. Neutral and Charged Inter-Valley Biexcitons in Monolayer $MoSe_2$. *Nat. Commun.* **2017**, *8*, 15552.
(11) Ye, Z.; Waldecker, L.; Ma, E. Y.; Rhodes, D.; Antony, A.; Kim, B.; Zhang, X.-X.; Deng, M.; Jiang, Y.; Lu, Z.; et al. Efficient Generation of Neutral and Charged Biexcitons in Encapsulated WSe_2 Monolayers. *Nat. Commun.* **2018**, *9*, 3718.
(12) Chen, S.-Y.; Goldstein, T.; Taniguchi, T.; Watanabe, K.; Yan, J. Coulomb-Bound Four- and Five-Particle Intervalley States in an Atomically-Thin Semiconductor. *Nat. Commun.* **2018**, *9*, 3717.
(13) Cadiz, F.; Courtade, E.; Robert, C.; Wang, G.; Shen, Y.; Cai, H.; Taniguchi, T.; Watanabe, K.; Carrere, H.; Lagarde, D.; et al. Excitonic Linewidth Approaching the Homogeneous Limit in MoS_2-Based van der Waals Heterostructures. *Phys. Rev. X* **2017**, *7*, 021026.
(14) Jones, A. M.; Yu, H.; Schaibley, J. R.; Yan, J.; Mandrus, D. G.; Taniguchi, T.; Watanabe, K.; Dery, H.; Yao, W.; Xu, X. Excitonic Luminescence Upconversion in a Two-Dimensional Semiconductor. *Nat. Phys.* **2016**, *12*, 323−327.
(15) Jadczak, J.; Glazov, M.; Kutrowska-Girzycka, J.; Schindler, J. J.; Debus, J.; Ho, C.-H.; Watanabe, K.; Taniguchi, T.; Bayer, M.; Bryja, L. Upconversion of Light into Bright Intravalley Excitons via Dark Intervalley Excitons in hBN-Encapsulated WSe_2 Monolayers. *ACS Nano* **2021**, *15*, 19165−19174. PMID: 34735768.
(16) Żuberek, E.; Majak, M.; Lubczyński, J.; Debus, J.; Watanabe, K.; Taniguchi, T.; Ho, C.-H.; Bryja, L.; Jadczak, J. Upconversion Photoluminescence Excitation Reveals Exciton-Trion and Exciton-Biexciton Coupling in *hBN*/WS_2/*hBN* van der Waals Heterostructures. *Sci. Rep.* **2022**, *12*, 13699.
(17) Hao, K.; Xu, L.; Nagler, P.; Singh, A.; Tran, K.; Dass, C. K.; Schüller, C.; Korn, T.; Li, X.; Moody, G. Coherent and Incoherent Coupling Dynamics between Neutral and Charged Excitons in Monolayer $MoSe_2$. *Nano Lett.* **2016**, *16*, 5109−5113. PMID: 27428509.
(18) Jadczak, J.; Bryja, L.; Kutrowska-Girzycka, J.; Kapuscinski, P.; Bieniek, M.; Huang, Y.-S.; Hawrylak, P. Room temperature multiphonon upconversion photoluminescence in monolayer semiconductor WS_2. *Nat. Commun.* **2019**, *10*, 107.
(19) Zipfel, J.; Wagner, K.; Semina, M. A.; Ziegler, J. D.; Taniguchi, T.; Watanabe, K.; Glazov, M. M.; Chernikov, A. Electron Recoil Effect in Electrically Tunable $MoSe_2$ Monolayers. *Phys. Rev. B* **2022**, *105*, 075311.
(20) Liu, E.; van Baren, J.; Lu, Z.; Taniguchi, T.; Watanabe, K.; Smirnov, D.; Chang, Y.-C.; Lui, C.-H. Exciton-Polaron Rydberg States in Monolayer $MoSe_2$ and WSe_2. *Nat. Commun.* **2021**, *12*, 6131.
(21) Yang, Q.; Xue, Y.; Chen, H.; Dou, X.; Sun, B. Photo-Induced Doping Effect and Dynamic Process in Monolayer $MoSe_2$. *Journal of Semiconductors* **2020**, *41*, 082004.
(22) Wang, G.; Palleau, E.; Amand, T.; Tongay, S.; Marie, X.; Urbaszek, B. Polarization and Time-Resolved Photoluminescence Spectroscopy of Excitons in $MoSe_2$ Monolayers. *Appl. Phys. Lett.* **2015**, *106*, 112101.
(23) Kioseoglou, G.; Hanbicki, A. T.; Currie, M.; Friedman, A. L.; Jonker, B. T. Optical Polarization and Intervalley Scattering in Single Layers of MoS_2 and $MoSe_2$. *Sci. Rep.* **2016**, *6*, 25041.
(24) Baranowski, M.; Surrente, A.; Maude, D. K.; Ballottin, M.; Mitioglu, A. A.; Christianen, P. C. M.; Kung, Y. C.; Dumcenco, D.; Kis, A.; Plochocka, P. Dark Excitons and The Elusive Valley Polarization in Transition Metal Dichalcogenides. *2D Materials* **2017**, *4*, 025016.
(25) Dery, H.; Song, Y. Polarization Analysis of Excitons in Monolayer and Bilayer Transition-Metal Dichalcogenides. *Phys. Rev. B* **2015**, *92*, 125431.
(26) Manca, M.; Glazov, M. M.; Robert, C.; Cadiz, F.; Taniguchi, T.; Watanabe, K.; Courtade, E.; Amand, T.; Renucci, P.; Marie, X.; et al. Enabling Valley Selective Exciton Scattering in Monolayer WSe_2 Through Upconversion. *Nat. Commun.* **2017**, *8*, 14927.
(27) Jeong, T.-Y.; Bae, S.; Lee, S.-Y.; Jung, S.; Kim, Y.-H.; Yee, K.-J. Valley Depolarization in Monolayer Transition-Metal Dichalcogenides With Zone-Corner Acoustic Phonons. *Nanoscale* **2020**, *12*, 22487−22494.
(28) Bae, S.; Matsumoto, K.; Raebiger, H.; Shudo, K.; Kim, Y.-H.; Handegard, O. S.; Nagao, T.; Kitajima, M.; Sakai, Y.; Zhang, X.; et al. K-Point Longitudinal Acoustic Phonons Are Responsible for Ultrafast Intervalley Scattering in Monolayer $MoSe_2$. *Nat. Commun.* **2022**, *13*, 4279.
(29) Song, Y.; Dery, H. Transport Theory of Monolayer Transition-Metal Dichalcogenides through Symmetry. *Phys. Rev. Lett.* **2013**, *111*, 026601.
(30) Ayari, S.; Jaziri, S.; Ferreira, R.; Bastard, G. Phonon-Assisted Exciton/Trion Conversion Efficiency in Transition Metal Dichalcogenides. *Phys. Rev. B* **2020**, *102*, 125410.
(31) Perea-Causin, R.; Brem, S.; Malic, E. Trion-Phonon Interaction in Atomically Thin Semiconductors. *Phys. Rev. B* **2022**, *106*, 115407.
(32) Christiansen, D.; Selig, M.; Berghäuser, G.; Schmidt, R.; Niehues, I.; Schneider, R.; Arora, A.; de Vasconcellos, S. M.; Bratschitsch, R.; Malic, E.; et al. Phonon Sidebands in Monolayer Transition Metal Dichalcogenides. *Phys. Rev. Lett.* **2017**, *119*, 187402.
(33) Castellanos-Gomez, A.; Buscema, M.; Molenaar, R.; Singh, V.; Janssen, L.; van der Zant, H. S. J.; Steele, G. A. Deterministic Transfer of Two-Dimensional Materials By All-Dry Viscoelastic Stamping. *2D Materials* **2014**, *1*, 011002.

https://doi.org/10.1021/acs.jpclett.3c01982
J. Phys. Chem. Lett. 2023, 14, 8702−8708